

Design proposal and feasibility analysis for a near-surface wave-powered profiling float

Russell Shomberg² Michael Jakuba^{1,*} Dana Yoerger¹

Abstract—We propose a design for a float capable of harvesting wave energy while fully submerged. The proposed design could theoretically operate indefinitely without ever breaching the surface. We developed and validated design guidelines for the proposed float through a combination of tank testing and simulation. These design insights could be employed to build an operational float. Our final proposed design utilizes a 0.91 m heave-plate and six 0.46 m turbines to generate 10 W across a range of simulated conditions.

¹ Woods Hole Oceanographic Institution, MA, USA

² University of Rhode Island, RI, USA

* Michael Jakuba <mjakuba@whoi.edu>

I. INTRODUCTION

This effort is an expansion of work presented at Oceans 2022 Hampton Roads [25] where a design concept for a near-surface wave energy converter (WEC) profiling float was proposed with simulations and tank testing to explore the feasibility of the concept. Here we expand on the methods used for tank testing, modeling, and simulations. Additionally, we propose a design methodology for the float and propose a final design with dimensions to be used in a future prototype.

Autonomous floats play an important role throughout the ocean sciences [12, 22, 21]. To extend deployments beyond battery life limitations, some floats employ environmental energy harvesting such as solar [22], wind [5], and wave [30] energy. Data buoys represent a small scale application for WECs [18].

Recent developments in wave power show that, for the scale of a scientific floats, oscillating body style WECs have the highest efficiencies [2]. Many oscillating body WECs harvest energy from the bobbing motion caused by buoyancy in oscillating flow for a semi-submerged body [10]. However, that design requires an exposed surface expression to create variable buoyant force. Two-body systems can employ a buoyant surface float to drive a power take-off (PTO) system far below in the relatively still water [30]. Drifting wave-energy harvesting robotic systems of this format have been shown to be capable of generating power [29], holding station [13], and traversing long distances [7].

Surface expressions are also not always feasible or desired due to environmental considerations. Extreme weather such as high winds or breaking waves can cause damage to fragile parts [16, 11]. Even at a small distance below the

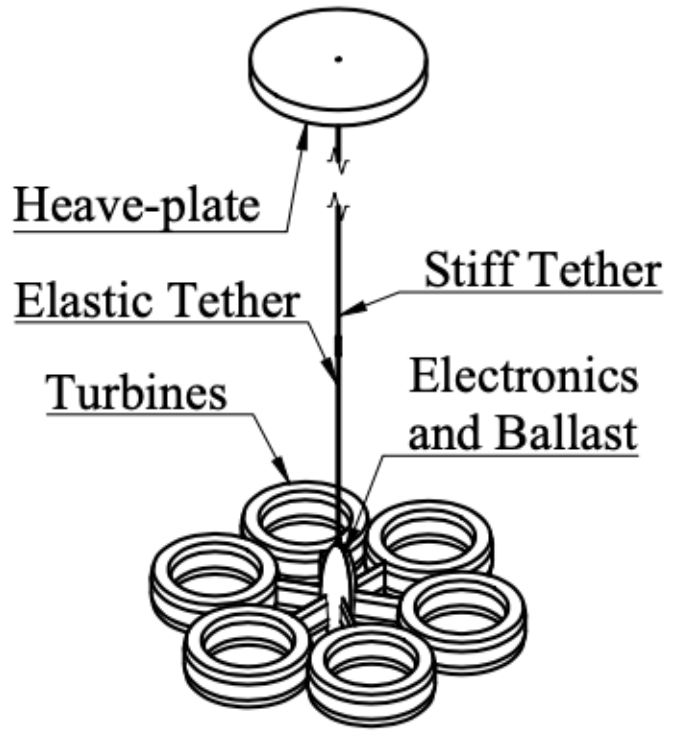


Fig. 1. Conceptual drawing of a proposed near-surface WEC design. The design consists of a buoyant heave-plate and ballasted electronics pod connected by a long partially elastic tether. An array of power-generating turbines is attached to the pod.

surface, a device can acquire significant protection from damage. Locations at high latitudes such as the Irminger Sea are often of high interest for observation [19] [17] [27]. Bio-fouling is also reduced at even a small depth from the surface. Unlike solar and wind, wave energy can be harvested from below the surface. However, existing free-floating WECs all rely on floating surface structures.

Additionally, without a surface expression, floats could operate without risk of detection. Such deployments may have data gathering applications for scientific, military, and industrial purposes. Military applications include of adversary-controlled waters. Scientific and industrial applications include locations at risk to theft or vandalism.

Currently, no examples exists of a fully submerged free-floating WEC. However, a wide body of research exists for both wave-powered floats [30] and submerged WECs [2]. Existing free-floating WECs rely on buoyancy forcing of

a semi-submerged body. Existing submerged WECs are generally fixed to the sea floor. In both cases, the existing designs rely on grounding either to the sea floor or surface.

Unlike conventional two-body WECs which rely on a surface expression to provide ground, the proposed design would operate without direct coupling to the surface motion and must instead harvest energy from the orbital velocity of the wave field. A submerged WEC must also overcome the exponential loss of wave energy with depth [28], so the device must operate close enough to surface to harvest the required energy. However, due to the unpredictable nature of ocean waves, the risk of a surface breach increases with proximity to the surface requiring an active control system.

Our proposed design (Fig. 1) exploits the difference in the orbital velocities between near-surface and deep water. The device operates entirely submerged. A heave-plate transmits near-surface wave forcing through the long tether into turbines attached to a negatively buoyant electronics pod. The pod's turbines generate power through the flow caused by the oscillations of the pod through the deep water where wave-driven orbital motion is attenuated. To control depth, the turbines vary PTO to vary system drag in sync with the pod velocity ratcheting the WEC up or down in water column.

Sizing of the proposed WEC depends on both power requirements and the expected wave environment. Depth control must be sufficient to avoid breaching while operating in proximity to the surface. Additionally, the device must be designed to avoid the tether going slack which would lower power generation and potentially cause damage from snap loads. A compliant tether could assist to damp out large oscillations without slacking and could also potentially exploit resonance.

This study explores the feasibility of the proposed design through experimental validation of a model, exploring design parameters, and finally developing optimization guidelines for a operational device. Based on power consumption of common floats [6, 4], a feasible device would likely need to produce power on the order of several of watts to charge a battery capable of powering the device. For example, assuming a float uses approximately 4 Wh per 10 day cycle [9], a WEC capable of harvesting just 1 W of power could recharge the battery in just 4 hours. A feasible design must generate sufficient power across a range of wave environments without breaching the surface or slacking the tether. Additionally, the dimensions of a feasible design must be build-able using commercially available materials.

We tested a prototype electronics pod which generated up to 1 W of power in tank tests with small scale waves while matching expected motion using a model with fitted coefficients. Through further model simulations, we develop a design process based on nondimensional parameters for creating feasible designs for different wave environments. We then use our design process to arrive at parameters for a full-scale device. We then analyze the performance of

the full-scale device in simulation to show adequate power generation and depth control across a range of wind speeds. Finally we report a potential design with major dimensions and simulation results showing feasibility of the proposed design in a range of wave environments.

II. SYSTEM OVERVIEW

The proposed design (Fig. 1) is a two body WEC with an upper heave-plate and lower pod with turbines that drive a PTO. The system is neutrally buoyant and operates with heave-plate just below the surface. The heave-plate experiences forcing from the near-surface wave-field which is transferred through the tether to the pod causing it to oscillate in the relatively still water below. These oscillations cause flow through the turbines which produces power. Turbine thrust resists pod motion and can be varied by varying the PTO. This variable drag can be exploited to control the depth of the device.

A. Wave Model

The design relies on wave forcing from the near-surface orbital velocity to harvest wave power.

Average potential wave power \mathcal{P}_w is defined per unit length of wave-crest L_c . For deep-water waves, wave power is a function (Eq. 1) of significant wave height H_0 and group speed c_g , determined by the energy period T_e for deep-water waves where ρ and g denote water density and gravitational acceleration respectively [23]. To limit the parameter space all simulations presented subsequently assume either a monochromatic or Pierson-Moskowitz (PM) spectrum [20]. The latter describes the theoretical spectrum for a fully developed open-ocean wave field with the principle advantage that it is parameterized by a single number, wind speed U_{10} (at 10 m above sea surface).

$$\begin{aligned} H_0(U_{10}) &\approx 0.22 \frac{U_{10}^2}{g} \\ T_e(U_{10}) &\approx 1.17 \frac{2\pi U_{10}}{g} \\ c_g &= \frac{g T_e}{4\pi} \\ \frac{\mathcal{P}_w}{L_c} &= \frac{1}{16} \rho g H_0^2 c_g \end{aligned} \quad (1)$$

Morison's Equation (Eq. 2) describes the oscillatory forces waves induce on bodies such as heave-plates [8, 3]. The force on a body F_b is dependent on the velocities of body v_b and the surrounding fluid v_f . The coefficients represent added mass C_a and vertical drag C_d , and the resulting force is the sum of the hydrodynamic inertial and drag forces which depend on body volume V_b and frontal area A_b respectively as well as the density of the fluid ρ and body ρ_b . For our effort, buoyancy B and weight W are balanced to cancel each other out.

$$\begin{aligned} F_b = & \rho_b V_b \dot{v}_b + \rho C_a V_b (\dot{v}_f - \dot{v}_b) \\ & + \frac{1}{2} \rho C_d A_b |v_f - v_b| (v_f - v_b) \\ & + B - W \end{aligned} \quad (2)$$

It can also be represented (Eq. 3) using body mass m_b and hydrodynamic derivatives for added mass m'_b and drag Z . For thin-plate bodies ($m'_b \gg m_b$), mass can be ignored, further simplifying (Eq. 4) the forcing function.

$$F_b = m_b \dot{v}_f + m'_b (\dot{v}_f - \dot{v}_b) + Z_b |v_f - v_b| (v_f - v_b) \quad (3)$$

$$F_b \approx m'_b (\dot{v}_f - \dot{v}_b) + Z_b |v_f - v| (v_f - v) \quad (4)$$

To compare designs with different sized heave-plates, we used the Keulegan-Carpenter (KC) number. Additionally, a second KC number is used to describe scaling effects on each individual turbine. The KC number describes the relative importance of the drag forces over inertia forces for bluff objects in an oscillatory fluid flow [14].

$$KC = \frac{2\pi a}{L} \quad (5)$$

For bodies in an oscillating flow, KC is commonly simplified (Eq. 5) to only depend on wave amplitude $a = H_0/2$ and a characteristic length L represented here by the heave-plate diameter.

B. Force Model

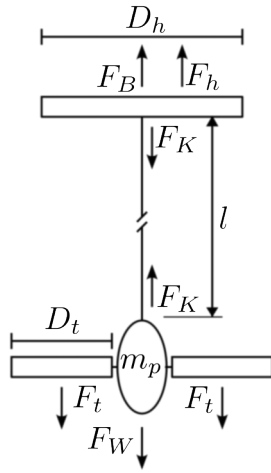


Fig. 2. Simplified free body diagram showing major dimensions and forces on the near-surface WEC. The system consists of a buoyant heave-plate of diameter D_h attached via a long tether of length l to a ballasted pod of mass m_p with turbines of diameter D_t . For neutrally buoyancy, the total weight F_W is counteracted by the total buoyancy F_B . The tether holds tension F_K . Oscillating waves impart heave force F_h and PTO from the turbines creates a resistive thrust F_t . Here, parasitic drag force is ignored under the assumption that pod diameter is much smaller than turbine diameter.

The force model (Fig. 2) shows how the wave forcing on the heave-plate is counteracted by pod inertia and turbine

resistive thrust through tension in the tether. The model relies on a tether of sufficient length to ensure the turbines operate below the wave-field.

C. System Elements

1) *Heave-Plate*: Heave-plate forcing from vertical waves is described by Morrison's equation (Eq. 4) where the added mass and drag coefficient are modeled from a thin disc ($C_a = 1, C_d = 1.2$) or determined empirically.

$$m'_h = \rho \frac{D_h^3}{3} \quad (6)$$

$$Z_h = \frac{1}{2} C_d \rho \frac{\pi D_h^2}{4} \quad (7)$$

Overall system buoyancy F_B primarily comes from the heave-plate and depends on plate thickness. As the thickness increases, the thin-disc assumption loses validity.

2) *Ballast Mass*: The electronics pod including the turbine housings is modeled as a point mass m_p with all inertia associated with the pod and turbines incorporated into this single value.

Overall system weight F_W is primarily determined by ballast mass and must counteract system buoyancy F_B . However, buoyancy can also be added to the lower body to help ballast the system.

3) *Elastic Tether*: The elastic tether is modeled as a linear spring (Eq. 8) with stiffness K . Spring force depends on change in length ($F_K = K\Delta l$).

$$F_K = K\Delta l \quad (8)$$

The opposing forces of heave-plate buoyancy and pod weight determine the equilibrium tether tension and length. The tether force F_K is taken as the offset from equilibrium and negative values of greater magnitude than the equilibrium tension are recognized as tether slackening events.

The tether can be made of a stiff and flexible section, but the device can access significant energy only from waves for which the overall tether length exceeds their spatial wavelength (inverse wave number).

4) *Turbines*: turbine resistive thrust is based on the PTO (Eq. 9) which can be adjusted electronically by a controller. Total turbine area nA_t depends on individual diameter D_t and number n of turbines. Actual area and number of individual turbines will affect individual turbine KC number and parasitic drag. While more efficient, lower KC numbers representing fewer larger individual turbines indicate a system dominated by inertial forces associated with accelerating fluid, whereas typical turbines operate in constant velocity flows. Maximum theoretical PTO is a function of the maximum power coefficient C_p which is given by the Betz limit ($C_p = 16/27$) [15] or measured empirically for a specific turbine. Turbine resistive thrust F_t resists pod velocity v_p contributing to overall drag. The turbine resistive thrust depends on the thrust constant Z_t .

$$\mathcal{P}_t = F_t v_p = \frac{1}{2} n \rho C_p A_t |v_p|^3 \quad (9)$$

$$F_t = \frac{1}{2} \rho n C_p A_t |v_p| v_p \quad (10)$$

$$Z_t = \frac{1}{2} n \rho C_p A_t \quad (11)$$

D. Control

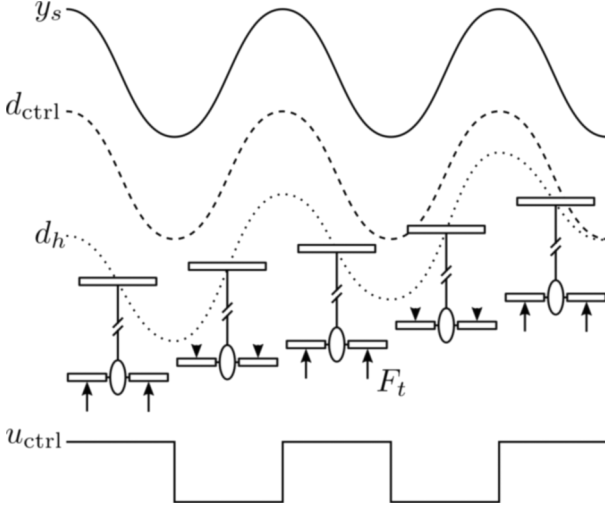


Fig. 3. Concept drawing for a PTO based bang-bang controller. The control signal u_{ctrl} is a function of pod velocity v_p and depth error ($d_{ctrl} - d_h$). It alternates between high and low modulating turbine PTO and therefore thrust F_t represented by arrows showing direction and magnitude. By default, the signal is high. However when the pod velocity v_p is in the opposite direction as depth error defined by instantaneous depth d_h below the surface y_s compared to a set control depth d_{ctrl} , the PTO is minimized to reduce drag increasing movement in the corrective direction.

The system can be controlled using a control signal u_{ctrl} to modulate (Eq. 12) the turbine PTO and therefore thrust. One possible implementation consists of a bang-bang controller switches the control signal between 0 and 1 as a function of depth error ($d_{ctrl} - d_h$) and pod velocity v_p .

$$F_t = u_{ctrl} n Z_t |v_p| v_p \quad (12)$$

The design changes depth using a ratcheting effect by modulating PTO in sync with pod velocity. Lowering the PTO reduces system drag preserving more overall momentum in the instantaneous direction of pod velocity. The control depth will be chosen to maximize power generation under an acceptable risk of surface breaching.

E. Dynamic Model

The system dynamics (Fig. 4) represent a non linear system (Eq. 13) with state variables tether tension F_K , pod velocity v_p and relative wave-field to heave-plate velocity v_{sh} . The only input is wave-field velocity $v_f(t, d_h)$. For the control signal u_{ctrl} , we added the heave-plate depth $d_h = \int v_{sh} dt$.

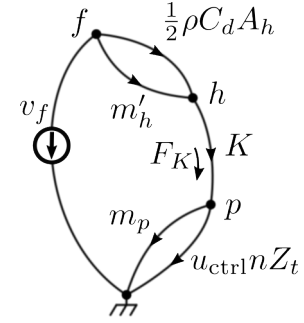


Fig. 4. System represented as a system graph [24]. The nodes represent the velocity v of the wave-field f , heave-plate h , pod p , and ground (still deep water). The edges represent forces imparted by relative motion. The oscillating wave-field is represented by a velocity source v_f . Surface motion relative to the heave-plate v_{sh} imparts hydrodynamic forces from added mass m'_h and drag constant Z_h . Heave-plate motion relative to the pod v_{hp} creates tension F_K from the tether stiffness K . The pod motion v_p is resisted by inertia from mass m_p and thrust from the n turbines based on thrust constant Z_t modulated by the control signal u_{ctrl} .

$$\begin{bmatrix} \dot{F}_K \\ \dot{v}_p \\ \dot{v}_{sh} \\ \dot{d}_h \end{bmatrix} = \begin{bmatrix} -K[v_p + v_{sh}] + Kv_f(t, d_h) \\ \frac{F_K}{m_p} - u_{ctrl}(d_h, v_p) \frac{n Z_t}{m_p} |v_p| v_p \\ \frac{F_K}{m'_h} - \frac{1}{2} \frac{C_d \rho A_h}{m'_h} |v_{sh}| v_{sh} \\ v_{sh} \end{bmatrix} \quad (13)$$

Instantaneous power output \mathcal{P}_o is determined by flow through the turbines and a power coefficient C_p . In theory, the power coefficient is equal to the thrust constant (Eq. 11), but additional loss can be expected based on efficiency η . ($C_p = 16/27$ is the theoretical upper limit for turbine PTO). The power coefficient can be modulated electronically using a control signal u_{ctrl} which also modulates the thrust and therefore overall system drag.

$$\mathcal{P}_o = \eta u_{ctrl} \frac{1}{2} \rho C_p n A_t |v_p|^3 \quad (14)$$

The system is a double-ended quadratically damped harmonic oscillator. Depending on the parameters, the system could be broadband, resonant, or anti-resonant. However, due to quadratic damping, the system can only be under-damped [26].

III. TANK TESTING

We conducted tank tests to validate our mathematical model, explore the design space related to system resonance, and show the feasibility of generating power and control from the oscillating turbines on an elastic tether. For the tests, a prototype pod was suspended in a vertical test tank and oscillated using a custom built testing apparatus (Fig. 5) designed to simulate, through force-feedback, the effect of suspending the pod beneath the heave-plate using an elastic tether.

We conducted tank tests to validate our mathematical model, to explore the design space related to system resonance, and to show the feasibility of power generation

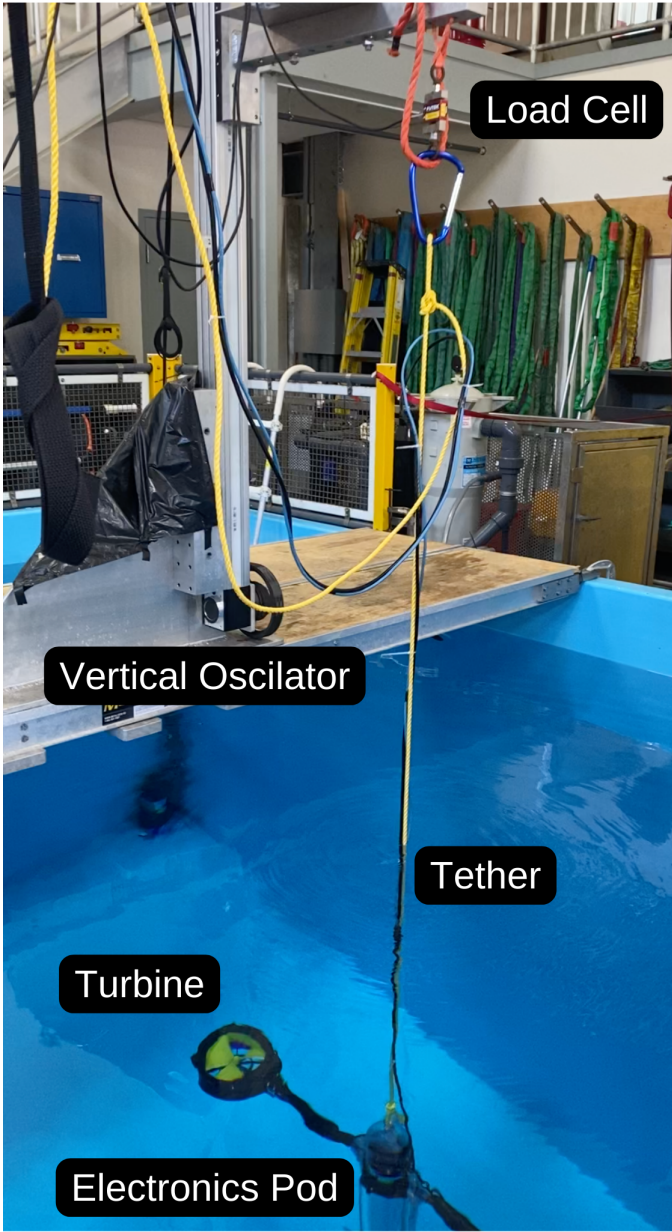


Fig. 5. A prototype version of the electronics pod and two turbines is suspended in the water from a custom vertically oscillating apparatus. A force sensor provides feedback allowing the apparatus to mechanically simulate the tether force calculated from both the prototype pod movement and virtual surface heave. The apparatus tests the prototype's dynamic response and power generation from different input waves across a range of tether stiffnesses.

and depth control of the concept. For the tests, a prototype pod was suspended vertically in the test tank and oscillated using a custom-built apparatus (Fig. 5) designed to simulate, through force-feedback, the effect of suspending the pod beneath the heave-plate on an elastic tether in a wave field.

A. Testing Apparatus

We designed and fabricated an experimental apparatus (Fig. 5) consisting of a Bosch 4 m vertical slide driven by a 5 hp Clearpath servo motor with the pod or various test

articles suspended below in a 4 m deep tank at WHOI. Initially the device was commanded to follow a closed-loop position trajectory, either a monochromatic wave-form or a realization of the PM spectrum. These tests simulated an inextensible tether. Physical springs of sufficiently low elasticity to excite resonance proved unworkably long. To simulate the effect of an elastic tether, we instead measured vertical force on the pod and fed the result into a controller that issued torque commands to the motor.¹

A load cell between the sliding stage and a stiff polypropylene rope attached to the submerged device provided the measurement of vertical force on the pod.

The essential idea was to mimic the effect of a physical spring by closing the loop on force such that the measured force F_{meas} was driven to the theoretical (desired) force F_d created by a virtual linear spring between the virtual surface, specified as a time-varying waveform $z_s(t)$, and the actual, measured pod depth z :

$$F_d = k_s(z - z_s),$$

where k_s denotes a spring constant altered in software for each experiment.

A naive implementation of the controller would command motor torque τ_{motor} according to

$$\tau_{\text{motor}} = K_p(F_{\text{meas}} - F_d),$$

where K denotes a proportional gain that also captures the mechanical conversion between motor torque and the force applied to the stage. Actual implementation required compensating for preload, inertia, and non-linear Coulomb friction in the apparatus and attenuating control action at high frequencies to avoid exciting structural resonances in the physical system.

B. Prototype Pod

A prototype pod was suspended in the vertical tank from a load cell on the test apparatus arm as seen in (Fig. 5). The prototype consists of an aluminum frame holding a cylindrical electronics housing and ballast. The frame has two arms, each supporting a WaterLily Turbine.² WaterLily turbines were selected for the tests for convenience. Designed for generating power from flow in small streams, the turbines are commercially available, waterproof, and optimized for low flow rate operations. The three phases of each turbine were connected to a electronic commutation circuit that included the ability to duty cycle the combined output between open-circuit and across a resistor. Power across the resistor was measured throughout testing. To alter the PTO, the duty cycle could be altered between 100% and 0%, with 100% corresponding to maximum PTO

¹At the time, Clearpath's API did not provide access to their inner-most current/torque loop in the SC series of software controlled motors; however, with Clearpath's help, and because our system is pre-loaded, we were able to achieve the desired effect by continuous alteration of the torque/current limit.

²<https://www.waterturbine.com/>

somewhat below peak and 0% corresponding to minimum PTO. Maximum power generation is expected to occur between these extremes, however, in this work we consider a bang-bang controller switching between only maximum and minimum drag. Greater power output may have been possible using a maximum power-point tracking algorithm [1].

C. Testing Procedure

All tests, used the same prototype and the virtual surface input was a consistent monochromatic spectrum. Wave amplitude was limited by the height of the tank and amplitude gain at resonance. The spectrum had wave height 0.4 m and period 3.0 s corresponding to the wave energy period and significant wave height of a PM spectrum at a wind speed of 4 m s⁻¹ and a theoretical wave power of 235 W m⁻¹. Using the PTO duty cycles, tests were performed with the turbines at maximum and minimum (free-wheeling) resistance. For each configuration, we tested the prototype across a range of virtual tether stiffnesses representing designs with different natural frequencies including values significantly above and below the forcing frequency.

D. Tank Test Model

For the purpose for tank testing, we simplified the model to ignore heave-plate dynamics and assumed perfect coupling between the heave-plate and surface heave (Eq. 15) resulting in a somewhat higher power output than the same prototype would operating with a real heave-plate. Model input is the heave velocity v_h which is a function of time t based on the wave spectrum.

The simplified model has two additional parameters: pod added mass m'_p and pod (parasitic) drag constant Z_p . This differed from the base model (Eq. 13) where pod mass and added mass are lumped together and parasitic drag is assumed to be insignificant. However, the prototype has a relatively small turbines compared to pod size resulting in significant parasitic drag. Additionally, the model input is heave-plate velocity v_h as a function of time t which is assumed to perfectly track the wave-field. The modified equation of state

$$\begin{bmatrix} \dot{F}_K \\ \dot{v}_p \end{bmatrix} = \begin{bmatrix} K[v_p - v_h(t)] \\ \frac{F_K}{m_p + m'_p} - \frac{nZ_t + Z_p}{m_p + m'_p}|v_p|v_p \end{bmatrix}. \quad (15)$$

The state model can be integrated and rearranged (Eq. 16) into the format of a quadratically damped harmonic oscillator.

$$\ddot{y}_p + \frac{nZ_t + Z_p}{m_p + m'_p}|y_p|y_p + \frac{K}{m_p + m'_p}y_p = \frac{K}{m_p + m'_p}y_h(t) \quad (16)$$

TABLE I
PROTOTYPE POD PARAMETERS FITTED FROM TEST RESULTS.

Description	Symbol	Value	Units
Pod Mass	m_p	21.72	kg
Pod Added Mass	m'_p	5.85	kg
Turbine Thrust Constant	nZ_t	1.21	N s ² m ⁻¹
Pod (parasitic) Drag Constant	Z_p	28.78	N s ² m ⁻¹
Pod wet-weight	m_p	206.83	N
Power coefficient	C_p	0.13	-
Power Conversion Efficiency	η	0.51	-

E. Test Results

The system was tested with a single pair of turbines across a range of tether stiffnesses to determine the effects of resonance. Tests conducted at the maximum and minimum turbine drags show controllability potential. High drag tests were conducted at maximum power-takeoff while low drag tests were conducted with free-wheeling turbines. Comparison simulations use the fitted drag and added mass coefficients.

Parameters (Table. I) were fit across a full run of tests including multiple tether stiffnesses using Eq. 17,18. Tether force F_K is derived from Morison's equation (Eq. 2) to include pod mass and parasitic drag while assuming no fluid velocity. The first tank run was performed with the turbines freewheeling $Z_t = 0$ to isolate added mass m'_p and parasitic drag Z_p . For the second run, turbines were set to high PTO to determine the influence of turbine resistive thrust Z_t . The measured power output \mathcal{P}_o depends on the power conversion efficiency η parameter describes losses from the conversion of mechanical turbine power to electrical power across the prototype circuitry. Pod mass m_p was measured in air and used to calculate the other parameters. All of the coefficients are susceptible to over fitting due to the limited data set. To mitigate over fitting, we fitted to the entire data set rather than individual runs.

$$F_K = (m_p + m'_p)\dot{v}_p + (nZ_t + Z_p)|v_p|v_p \quad (17)$$

$$\mathcal{P}_o = \eta(nZ_t|v_p|^3) \quad (18)$$

The two WaterLily turbines have a diameter 150 mm resulting in a total turbine area of 0.0353 m². Based on the fitted thrust constant, these turbines have a power coefficient, calculated from Eq. 11, C_p significantly below the Betz limit. The power conversion efficiency η further reduces the power output.

The the model (Eq. 15) was then simulated using fitted coefficients (Tbl. I) and the same input heave velocity $v_h(t)$ from each run to compare how the model matched the measured results. An example (Fig. 6) from the tank testing showing a single tether stiffness K of the high PTO run shows a close match between simulated and measured results which is consistent throughout the tests. In all tests, measured turbine power slightly lags the simulated results and the velocity. This is likely due to the high rotational inertia of the test turbines which place the

rotating magnetic coil in the turbine rim. Additionally, the measured power results are asymmetric, showing greater power generation for positive velocity, likely due to the turbine ducting which is designed for single directional flow.

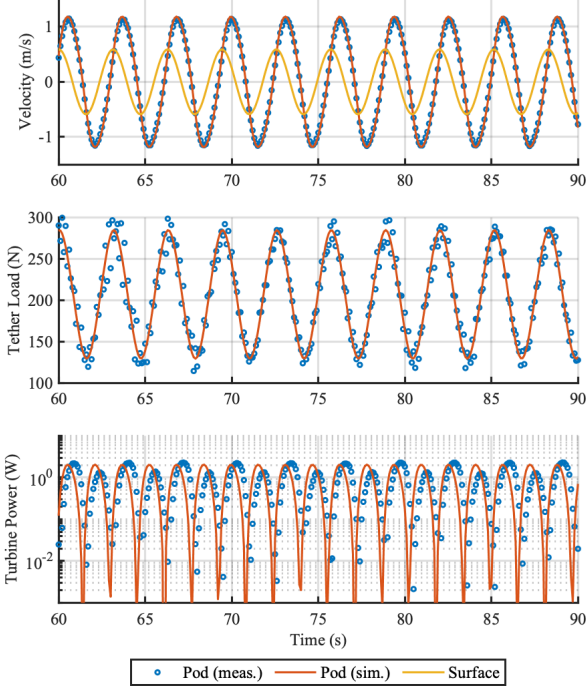


Fig. 6. Example results from an tank test run showing the pod motion and power generation. The example run was conducted with PTO set high and a virtual tether stiffness of 150 N/m, close the resonant peak of the system. The simulated results from the fitted coefficients match the measured values for position, force, and power. The input is a monochromatic wave spectrum of wave height 0.4 m and period 3.0 s

The results from the tank tests (Fig. 7) show a resonant peak for both power and gain observed at a tether stiffness around 150 N/m. At lower stiffnesses, gain and power drop off quickly to zero, while at higher stiffnesses, both gain and power appear to converge with gain approaching one as expected. When plotted against turbine KC number, gain and power become linear and quadratic respectively. Across all tests, the results show the close correlation between the simulated results and the measured results. However, the tests showed higher gain than expected by the simulations especially at resonance.

The tank tests validated the technique of fitting pod and turbine characteristics to our simplified model to predict a dynamic response and power generation. However, the tests were limited to a single prototype design under small wave amplitudes limited by the height of the tank. The tests also used the simplified model (Eq. 15) which does not take into account the heave-plate's impact on both power conversion and control. The large parasitic drag of the prototype significantly impacted the power generated; however, the power generated was measurable, and

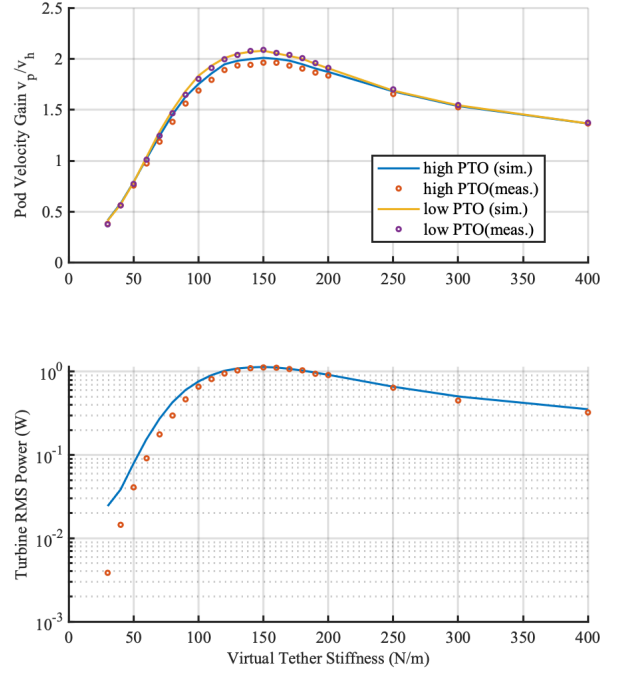


Fig. 7. Summary results from tank testing of the prototype pod at various virtual tether stiffnesses: (top) the ratio of pod oscillation amplitude to virtual surface amplitude; (bottom) RMS power generated with turbines at maximum resistance. Resonance occurs at virtual stiffnesses near 150 N/m, with steep decrease for more elastic springs and relatively modest decrease for stiffer springs. Varying PTO between 0% and 100% duty cycle had a small but measurable impact on amplitude ratio, indicating a degree of potential control authority. Comparison simulations use fitted drag and added mass coefficients. No power is generated for 0% duty cycle and no intermediate duty cycles were tested.

corresponded well to predictions from model, suggesting that further development of a deployable system could be carried out analytically and in simulation.

IV. SIMULATION RESULTS

A. Approach

To evaluate a wider range of design parameters consisting of tether stiffness, pod mass, total turbine area, and heave-plate diameter, we used simulations of the dynamic model (Eq. 13). Inclusion of the heave-plate dynamics increases model complexity compared to the tank tests. This complexity is important to capture because the imperfect surface tracking of the heave-plate contributes to both power conversion and controllability.

We simulated 5000 uniformly randomly selected parameter sets using the dynamic model (Eq. 13) developed earlier. Simulations set maximum turbine PTO to the Betz limit along with other simplifying assumptions and therefore present a best case for power output. We used parameter value ranges beyond reasonable limits to ensure we captured extrema for the model. Simulations were forced with a monochromatic wave-field having the same significant wave

height and energy period as a PM spectrum of equivalent wind speed. The initial simulations were limited to monochromatic spectrum at a single wind speed (8 m s^{-1}). Selected designs were also simulated across a range of wind speeds and using a full PM spectrum to confirm performance in a more realistic environment.

The simulations use a bang-bang controller (Fig. 3) which defaults to full power take-off except when the turbines are moving in the opposite direction as heave-plate depth error ($E_h = d_{ctrl} - d_h$). For all simulations the device starts with the heave-plates at the surface and the controller is given a desired depth d_{ctrl} equal to the significant wave height of the wave spectrum. Devices unable to exert any control remain at the surface.

B. Non-dimensionalized Results

Summary results from all simulations are presented (Fig. 8) in nondimensional form. The independent nondimensionalized design parameters (discussed separately below) are the frequency ratio, the heave-plate KC number, a drag ratio of turbines to heave-plate, and a mass ratio between pod mass and heave-plate added mass. Several examples (Tbl. II) to be discussed in more detail are marked on the plots.

The system can be described by just three of these non-dimensional ratios. However a fourth is shown as these values all represent physically understandable relationships between the design and environment as well as the designs of the upper and lower bodies. Descriptions of the four non-dimensional ratios follow.

1) *Frequency Ratio:* The ratio of a design's natural frequency of oscillation to the inverse of the wave period is given by $(2\pi/T_e)/(\sqrt{K/M})$. We will refer to this quantity as the frequency ratio for the sake of brevity. Power extraction efficiency shows a peak at resonance. At frequencies above resonance the power extraction efficiency falls off very quickly. Some broadband devices are able to produce high power but slacking is common in this region. Resonance also decreases controllability due to the phase delay reducing time where the turbines can effectively exert control.

2) *KC Number:* The heave-plate KC number, given by $\pi H_0/D_h$, is a comparison of the inertial versus drag forces on the heave-plate. Excessively high KC numbers, representing undersized heave-plates, cause power extraction efficiency to drop off quickly because small heave-plates experience less wave forcing. Excessively low KC numbers, representing oversized heave-plates, track the surface too well due to increased wave forcing for control to be effectively exerted by the turbine resistive thrust. Lower KC numbers also experience increased risk of tether slacking. The imperfect surface tracking of smaller heave-plates may provide additional damping for large wave oscillations.

3) *Drag Ratio:* The turbine to heave-plate drag ratio, given by $\frac{nZ_t}{(1/2)\rho C_d A_h}$, compares total turbine resistive thrust to heave-plate drag. Controllability depends heavily on this ratio. Excessively high drag-ratios, representing oversized

turbines, fail to produce power because the high drag stifles the motion required to generate flow for power generation. Excessively low drag ratios, representing undersized turbines, also fail to generate power, and are unable to exert control over a large heave-plate. Exceptions exist including Ex. 2 which are all highly resonant designs which are sensitive to design parameters and therefore likely difficult to build. Effective turbine area can be reduced by electronically decreasing power-take-off.

While drag ratio could be further simplified to an drag ratio, the drag ratio more accurately represents the physical realities by incorporating the drag and power coefficient into the nondimensional parameters allowing comparisons across turbine designs.

4) *Mass Ratio:* The mass ratio m_p/m'_h compares pod inertia to heave-plate inertia. Excessively high mass ratios, representing undersized heave-plates compared to device size, produce little power or control since the large pod inertia is not significantly affected by heave-plate forcing. Excessively low mass ratios, representing undersized pod masses, cause the pod to have little effect on the dynamics of the system unless the turbine resistive thrust is very large. These designs only generate significant power and control when operating as drag-dominated broadband devices and are susceptible to tether slacking.

We evaluated the simulations based on the RMS power extraction efficiency $\langle \mathcal{P}_o \rangle / \mathcal{P}_w$ and an RMS error ratio $\langle E_h \rangle / H_0$ of depth error to significant wave height. In all cases, power extraction efficiency values are low. Therefore system must rely on the high energy density of waves. The error ratio represents the inability of a design to achieve and maintain depth control. Since the control depth for each simulation is set equal to the significant wave height, an error ratio of $\langle E_h \rangle / H_0$ represents a completely uncontrollable device. We disregarded simulations where the tether went slack at any point as invalid.

C. Parameter Optimization

Using the nondimensional relationships shown as point clouds (Fig. 8), we are able to gain insight into the individual and combined effects of each design parameter. In particular, the upper edge of the power-gain point cloud and the lower edge of the error ratio cloud, show the best case given a set value for the corresponding parameter assuming all other parameters are well chosen. Even one relationship being poorly balanced could result in a design unable to generate power or control.

Once the nondimensional parameters are chosen, we can solve for the dimensional parameters for a given wave environment defined by the wind speed.

To select dimensional design parameters for a device we first calculate significant wave height H_0 and energy period T_e for the target wind speed. Then we use these environmental parameters and the chosen nondimensional parameters to solve for dimensional parameters. Finally, a real device can

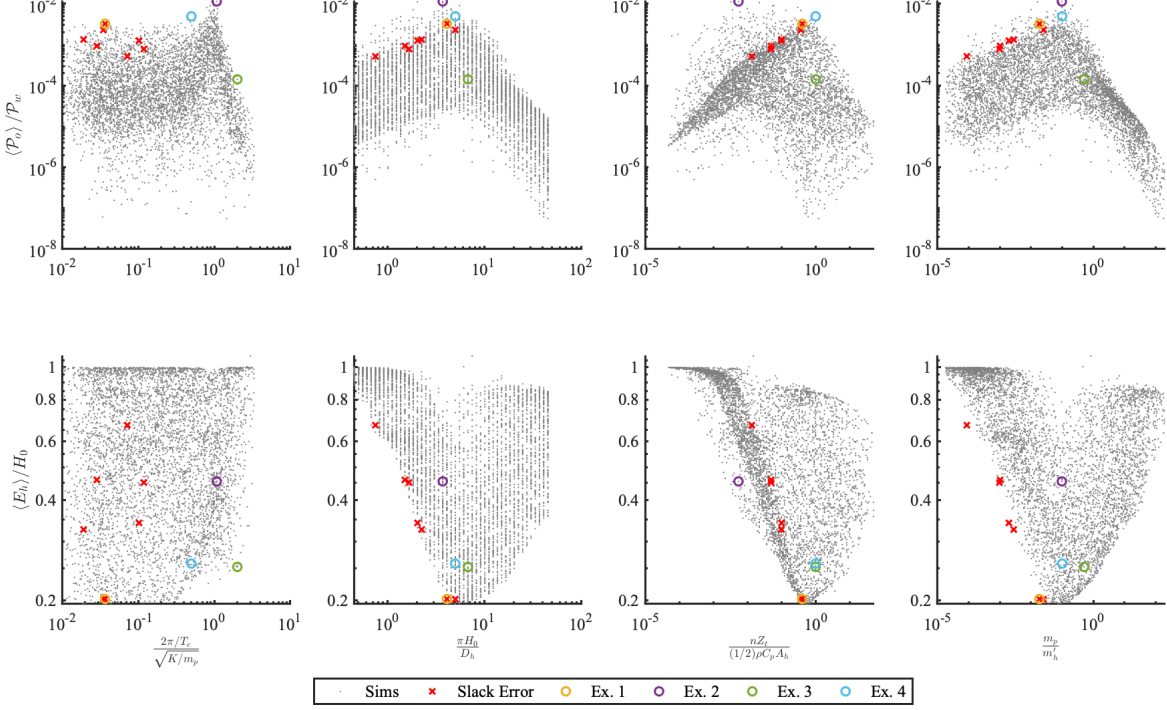


Fig. 8. nondimensional analysis of simulation results using monochromatic spectra. The point clouds represent possible realizations of the the parameter sets and simulation outputs. Points representing simulations which experienced slack events are represented in red. The output parameters are power extraction efficiency $\langle P_o \rangle / P_w$ and a depth error ratio to significant wave height $\langle E_h \rangle / H_0$. Input parameters are the ratio of the natural frequency to the wave frequency, heave-plate KC number, a turbine to heave-plate drag ratio, and a ratio of pod mass to heave-plate added mass. Slacking events can be seen concentrated in certain parameter values such as higher powered broadband devices. Ex. 1-4 represent, in order, examples of a broadband, resonant, anti-resonant, and weakly-resonant designs captured by the simulations.

be designed to meet the target parameters. This design process relies on simulation results produced using the simplified lumped-parameter dynamical model and with turbines operating at the Betz limit described in II. We return to a consideration of the validity of this approach after presenting examples of its application.

The example designs are representative of the different responses to forcing. The anti-resonant example produces little power or control in simulation. Both broadband and resonant designs are can be made viable. They each appear in separate regions of each point cloud (Fig. 8) and display different behaviour in the time series data (Fig. 9).

Ex. 1: Broadband Design Results: In the broadband example, the pod oscillates with the same magnitude and phase as the heave-plate. The device is closely matched to surface wave oscillations but is able to quickly reach and maintain the control depth. The tether force is closely matched to the turbine force but also undergoes some rapid oscillations especially around control signal changes where the turbines rapidly change thrust. The broadband design relies on large turbines and a small ballast allowing very responsive control and good power generation without large oscillations. However, the system is prone to slacking due to the small pre-load caused by the small ballast. If operated in higher wind speeds or in a realistic wave spectrum, large

oscillations can cause excessive slacking resulting in snap loading and potential damage.

Ex. 2: Resonant Design Results: In the resonant example, the pod oscillates $\sim 90^\circ$ out of phase with the heave-plate and at a much greater magnitude. The heave-plate is closely matched to the surface wave oscillations, but the device is able to reach and stay near the control depth. Tether force is much greater than turbine resistive thrust and not significantly affected by control signal changes. Additionally, The tether compliance allows for significantly larger waves without slacking. The resonant design relies on small turbines and a large ballast allowing good power generation from large oscillations. The smaller turbines produce sufficient power and thrust through higher velocities. However, the influence of the controller is limited by the pod phase lag. As a result the heave-plate oscillates around the control depth and the turbines' PTO is set low for about half of the cycle.

Ex. 3: Anti-resonant Design Simulation Results: In the anti-resonant example, the pod oscillates $\sim 180^\circ$ out of phase with the heave-plate and at a much smaller magnitude. The heave-plate is closely matched to the surface wave oscillations, but the device is able to quickly reach and maintain the control depth. However, pod oscillations remain small resulting in insignificant power

TABLE II

PARAMETERS ASSOCIATED WITH SIMULATION EXAMPLES. EX. 1-3 WERE SELECTED AS THE HIGHEST POWER OUTPUT WITHIN THEIR RESPECTIVE REGIONS: BROADBAND, RESONANT, AND ANTI-RESONANT. THE NON-DIMENSIONAL DESIGN PARAMETERS ARE DEPENDENT ON THE DIMENSIONAL DESIGN PARAMETERS. HOWEVER, FOR EX. 4 NON-DIMENSIONAL DESIGN PARAMETERS WERE SELECTED INDEPENDENTLY BASED ON A DESIGN PROCESS DESCRIBED IN SEC. IV-C RESULTING IN DEPENDENT DIMENSIONAL DESIGN PARAMETERS.

Description	Symbol	Ex. 1	Ex. 2	Ex. 3	Ex. 4	Units
Dimensional Design Parameters						
Heave Diameter	D_h	1.11	1.22	0.67	0.91	m
Tether Stiffness	K	11053	90	22	175	N m ⁻¹
Turbine Area	nA_t	78.54	1.30	71.06	1.01	m ²
Pod Mass	m_p	13.50	95.12	81.85	39.89	kg
Non-dimensional Design Parameters						
Frequency Ratio	$\frac{2\pi/T_e}{\sqrt{K/m_p}}$	0.04	1.07	2.01	0.50	-
Heave KC	$\frac{\pi H_0}{D_h}$	4.10	3.71	6.76	5.00	-
Drag Ratio	nZ_t/Z_h	0.40	0.01	1.00	1.00	-
Mass Ratio	m_p/m'_h	0.02	0.10	0.51	0.10	-
Non-dimensional Performance Metrics						
Power Conversion Ratio	$\langle \mathcal{P}_o \rangle / \mathcal{P}_w$	0.0033	0.0114	0.0001	0.0049	-
Depth Error Ratio	$\langle E_h \rangle / H_0$	0.20	0.45	0.25	0.26	-

Ex. 4: Proposed Design Simulation Results: The nondimensional parameters for Ex. 4 (Tbl. II) were chosen manually to create a weakly-resonant design in order to find a good compromise between the broadband and resonant designs. Then the dimensional parameters were solved for using a wind speed of 8 m s⁻¹.

The results for the proposed design (Fig. 10) show the pod oscillating with a slight phase lag and at a slightly larger magnitude than the heave-plate. The heave-plate is closely matched to surface wave oscillations, but the device is able to reach and stay near surface depth. Compared to the resonant example, the proposed design only sets the turbine PTO low for a small portion of each cycle once close to control depth. The design also reaches control depth in fewer cycles than previous examples. Compared to the broadband example, the proposed design is significantly less prone to slacking due to the compliant tether.

When simulated across a range of wind speeds using PM spectra (Fig. 11), all four examples have peak energy extraction efficiency at 8 m/s. However, at higher wind speeds, efficiency is less important due to the general increase in available wave power. The anti-resonant design (Ex. 3) performs worst at all wind speeds, and the broadband design (Ex. 1) experiences tether slackening even at relatively low wind speeds. The strongly (Ex. 2) and weakly (Ex. 4) resonant designs have similar performance at higher wind speeds with slacking remaining rare. However, at lower wind speeds the weakly resonant design significantly outperforms the strongly resonant design for both power and control. For all four examples depth error increases significantly with wind speed potentially increasing the risk of a surface breach. The risk could be mitigated by setting a deeper control depth and relying on the greater depth penetration of wave power at higher wind speeds.

D. Additional Design Considerations

With the dimensional design parameters chosen, we can design each component to meet the chosen parameters. The

process may require multiple iterations based on materials, component sourcing, and other influences that could change the design parameters.

Turbines must be sourced which match the total turbine resistive thrust while minimizing parasitic drag. Multiple smaller turbines will operate at higher KC number relative to large turbines, which should align better with the quasi-steady state assumption made in our modeling but does not preclude the unexplored possibility of good performance in unsteady flows. Smaller turbines are less efficient, require more support structure producing more parasitic drag. Additionally, the number of turbines must be even to provide counter-rotating pairs to prevent the pod from spinning.

In our simulations, turbine drag and power conversion are defined by the Betz limit. Actual values must be determined empirically and will determine total turbine area and therefore number of turbines for the final design. More sophisticated control of turbine PTO, e.g. maximum power point tracking (MPPT) [1], could improve power extraction. However, such methods would require modification to accommodate the additional function of depth control. Finally, turbines should produce minimal resistive thrust while free-wheeling.

The pod consists of the electronics housing, turbines with mounts, and ballast. These components and their added masses contribute to the pod mass parameter. Additional ballast could be added as necessary. The wet-weight of the pod can be determined empirically or estimated. If the pod wet-weight is excessively high, buoyancy foam could be added to the pod to reduce the overall specific gravity. The pod will also have some parasitic drag which should be kept to a minimum. Measures such as hydrodynamic fairings will need to be taken to ensure a relatively streamlined profile.

While total tether length must be greater than the largest target wavelength based on wave energy period for deep

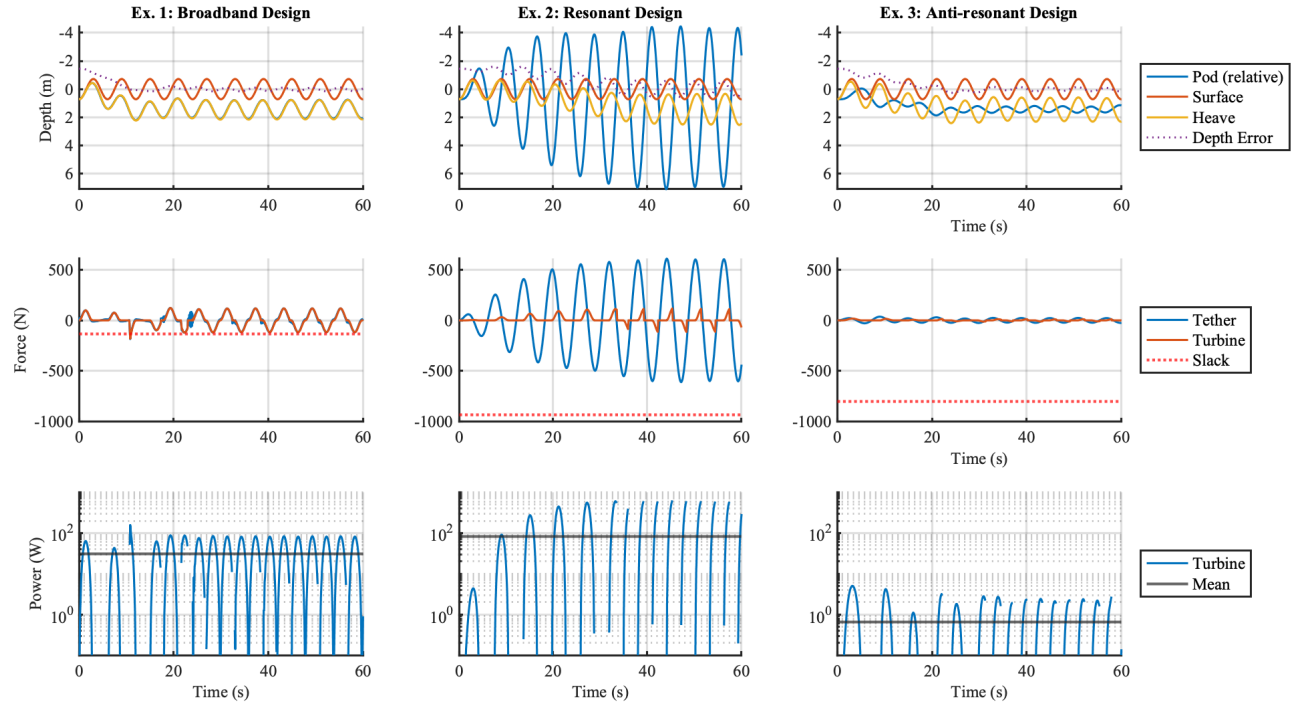


Fig. 9. Example simulation results for broadband, resonant, and anti-resonant designs, which correspond to the examples marked in Fig. 8, simulated in a monochromatic spectrum with a wind speed of 8 m s^{-1} . All simulations start with zero depth and have the control depth set to equal to the significant wave height. The resonant design produces the most power while the broadband design exerts the greatest control. However, the broadband design is more sensitive to cable slackening. The anti-resonant design performs poorly for both power and control.

water waves, the flexible section L of the tether can be shorter. An elastic material must be chosen with elastic modulus E and yield stress σ_y sized to cross-sectional area A and length L such that it provides the correct stiffness $K = EA/L$ without yielding under the maximum required tension $T_{\max} = \sigma_y A$. The maximum tension can be approximated from the simulations. The tether stiffness also determines the amount of pre-stretch in the tether.

Finally, the heave-plate must displace enough volume V_h to achieve neutral buoyancy for the entire device. The diameter is already fixed by the design parameters, so volume is proportional to thickness. The material density will determine the heave-plate wet-weight. For neutral buoyancy the total device wet-weight must be zero. The heave-plate may need to be structurally reinforced which could increase overall wet-weight and mass. Heave-plate thickness must be insignificant for the drag to be modeled as a flat plate. Otherwise the analysis will lose validity because an overly thick heave-plate will have different drag characteristics. Additionally, the simulations assume heave-plate mass to be insignificant compared to added mass based on it being a thin disk.

V. CONCLUSION

We developed a model for a novel design for a near-surface free-floating WEC and validated key elements of the design and our model for the full system using a turbine-

equipped prototype pod and purpose-built experimental apparatus. We developed a design process using a set of nondimensional parameters and proposed a feasible design.

The insights from this exploratory study suggest that an untethered autonomous float could be designed that harnesses near-surface wave power for extended operations. Enough power exists in the near-surface wave-field to power or recharge an autonomous float. The wave energy could be harvested using a submerged heave-plate in the oscillating wave-field tethered to an energy harvesting turbine hanging below in relatively still water. Such a device could exert control over its depth through temporally lowering PTO and therefore drag. A compliant tether allows such a device to exploit resonance for increased power extraction efficiency while also absorbing large wave fluctuations that might otherwise slack the tether and result in snap-loading. The study shows the considerations and relationships required for designing a device for a range of applications and conditions. It remains to develop and deploy an ocean-going prototype.

VI. ACKNOWLEDGMENTS

This project was made possible by the Office of Naval Research through a grant (N00014-16-1-3037). Russell Shomberg's participation in the project was funded by the Office of Naval Research NEPTUNE 2.0 Program (GRANT12941723). We wish to acknowledge Andrew

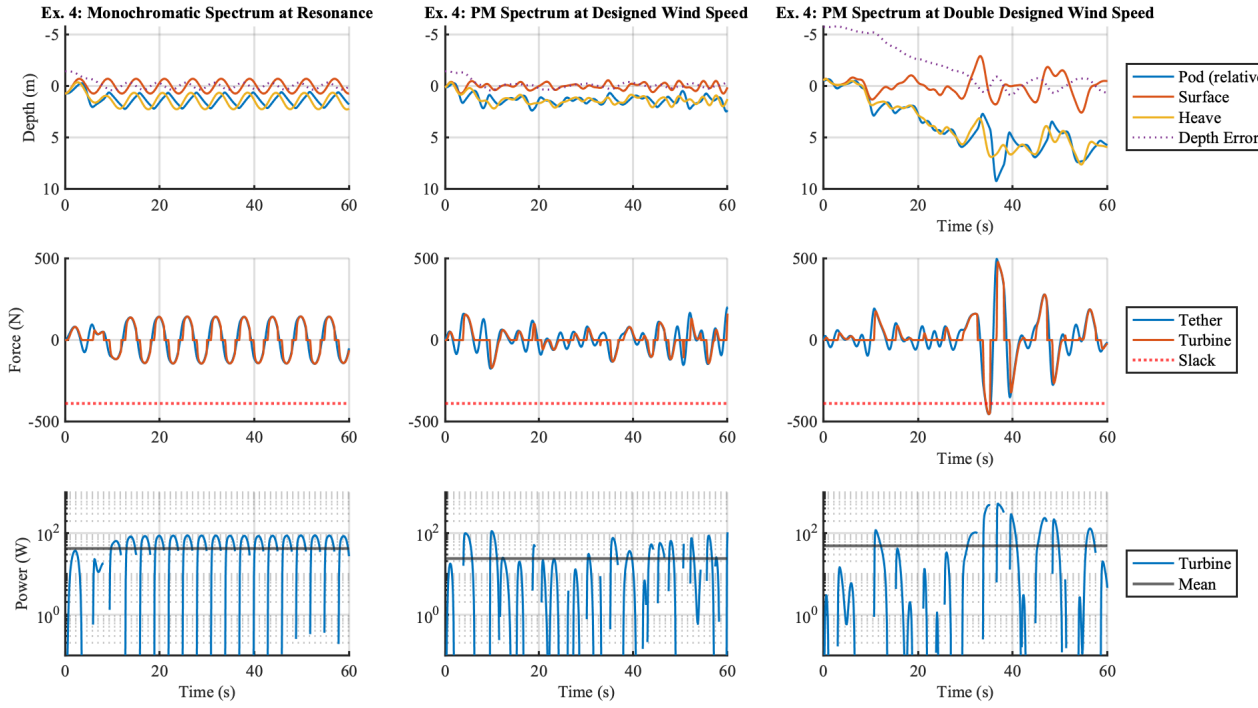


Fig. 10. Simulation results for the proposed design which corresponds to Ex. 4 marked in Fig. 8, simulated in a monochromatic spectrum and PM spectra both at and double the design wind speed of 8 m s^{-1} . All simulations start with zero depth and have the control depth set to equal to the significant wave height. The PM simulation at the design wind speed shows similar results to the monochromatic simulation. At elevated wind speeds, the design produces more power but less efficiently. Additionally, the elevated wind speed simulation can show some risk of tether slackening.

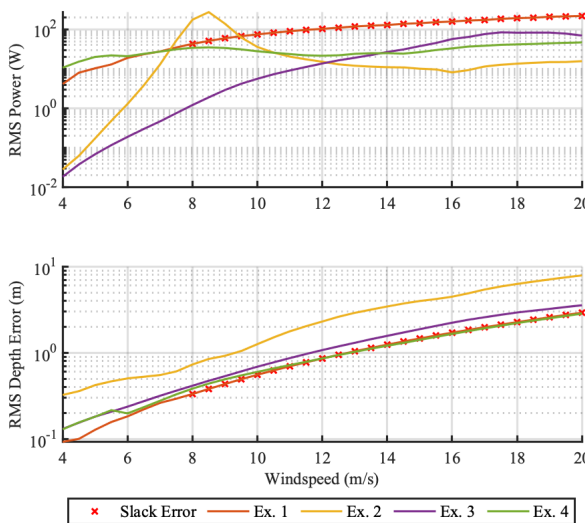


Fig. 11. Example designs compared across various wind speeds. Points representing simulations which experienced tether slack events are represented by a black 'X'. Ex. 1-4 represent, in order, examples of a broadband, resonant, anti-resonant, and weakly-resonant system captured by the simulations. The weakly-resonant system (Ex. 4) performs best for both power conversion and control for the widest range of wind speeds.

Billings, James Partan, Victor Naklicki, Jordan Stanway, and Jonathan Ware for their technical contributions to the project.

REFERENCES

- [1] Majid A Abdullah et al. "A review of maximum power point tracking algorithms for wind energy systems". In: *Renewable and sustainable energy reviews* 16.5 (2012), pp. 3220–3227.
- [2] Tunde Aderinto and Hua Li. "Review on power performance and efficiency of wave energy converters". In: *Energies* 12.22 (2019), p. 4329.
- [3] Adam Brown, Jim Thomson, and Curtis Rusch. "Hydrodynamic Coefficients of Heave Plates, With Application to Wave Energy Conversion". In: *IEEE Journal of Oceanic Engineering* 43.4 (2017), pp. 983–996. DOI: 10.1109/JOE.2017.2762258.
- [4] Robert J Cavagnaro et al. "Enabling marine energy integration for ocean observing: Functional requirements". In: *Global Oceans 2020: Singapore–US Gulf Coast*. IEEE. 2020, pp. 01–07.
- [5] Dezhong Chu et al. "2018 Unmanned Surface Vehicle (Saildrone) acoustic survey off the west coasts of the United States and Canada". In: *OCEANS 2019 MTS/IEEE SEATTLE*. IEEE. 2019, pp. 1–7.

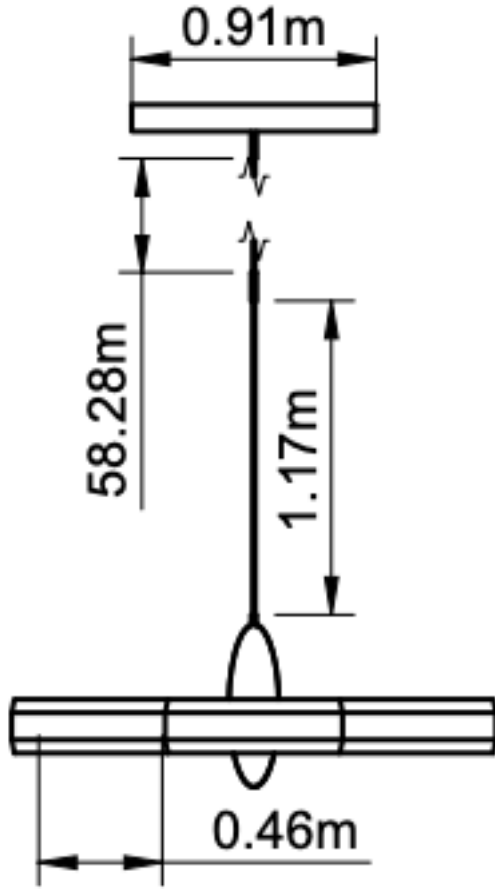


Fig. 12. Final proposed design with dimensions. The dimensions match Ex. 4 as shown in Tbl. II. From top to bottom, the dimensions represent, heave-plate diameter D_h , tether length for the stiff portion, tether length for the elastic portion, and turbine diameter D_t . The design has $n = 6$ turbines.,

- [6] Andrea E Copping et al. *Powering the Blue Economy-Ocean Observing Use Cases Report*. Tech. rep. Pacific Northwest National Lab.(PNNL), Richland, WA (United States), 2020.
- [7] Tom Daniel, Justin Manley, and Neil Trenaman. “The Wave Glider: enabling a new approach to persistent ocean observation and research”. In: *Ocean Dynamics* 61.10 (2011), pp. 1509–1520.
- [8] Jorgen Fredsoe and B Mutlu Sumer. *Hydrodynamics around cylindrical structures (revised edition)*. Vol. 26. World Scientific, 2006.
- [9] Lee Gordon. “Recommendations for reports about argo float batteries”. In: *University o f California San Diego (UCSD)* (2017).
- [10] Annette R Grilli et al. “Experimental and numerical study of spar buoy-magnet/spring oscillators used as wave energy absorbers”. In: *The Seventeenth International Offshore and Polar Engineering Conference*. OnePetro. 2007.
- [11] Martyn Hann, Deborah Greaves, and Alison Raby. “Snatch loading of a single taut moored floating wave energy converter due to focussed wave groups”. In: *Ocean Engineering* 96 (2015), pp. 258–271.
- [12] Steven R Jayne et al. “The Argo program: present and future”. In: *Oceanography* 30.2 (2017), pp. 18–28.
- [13] Hangil Joe et al. “Development of a flap-type mooring-less wave energy harvesting system for sensor buoy”. In: *Energy* 133 (2017), pp. 851–863.
- [14] Garbis H Keulegan and Lloyd H Carpenter. “Forces on cylinders and plates in an oscillating fluid”. In: *Journal of research of the National Bureau of Standards* 60.5 (1958), pp. 423–440.
- [15] Pierre Lecanu, Dominique Mouaze, Bertil Smorgrav, et al. “Theoretical Calculation of Wind (Or Water) Turbine: Extending the Betz Limit”. In: *Preprints* (2021).
- [16] SJ Lind, PK Stansby, and Benedict D Rogers. “Fixed and moored bodies in steep and breaking waves using SPH with the Froude-Krylov approximation”. In: *Journal of Ocean Engineering and Marine Energy* 2.3 (2016), pp. 331–354.
- [17] M Susan Lozier et al. “Overturning in the Subpolar North Atlantic Program: A new international ocean observing system”. In: *Bulletin of the American Meteorological Society* 98.4 (2017), pp. 737–752.
- [18] Iain McLeod and John V Ringwood. “Powering data buoys using wave energy: A review of possibilities”. In: *Journal of Ocean Engineering and Marine Energy* 8.3 (2022), pp. 417–432.
- [19] GWK Moore. “Gale force winds over the Irminger Sea to the east of Cape Farewell, Greenland”. In: *Geophysical Research Letters* 30.17 (2003).
- [20] Willard J Pierson Jr and Lionel Moskowitz. “A proposed spectral form for fully developed wind seas based on the similarity theory of SA Kitaigorodskii”. In: *Journal of geophysical research* 69.24 (1964), pp. 5181–5190.
- [21] Jean Rabault et al. “OpenMetBuoy-v2021: An Easy-to-Build, Affordable, Customizable, Open-Source Instrument for Oceanographic Measurements of Drift and Waves in Sea Ice and the Open Ocean”. In: *Geosciences* 12.3 (2022), p. 110.
- [22] RH Rozali et al. “Floating buoy technology for research purposes”. In: *Int J Innov Technol Explor Eng* 8.12 (2019), pp. 5514–5520.
- [23] Rick Salmon. “Introduction to ocean waves”. In: *Scripps Institution of Oceanography, University of California, San Diego* (2008).
- [24] J. Lowen Shearer, Arthur T. Murphy, and Herbert H. Richardson. *Introduction to System Dynamics*. Addison Wesley Publishing Company, Inc, 1967.
- [25] Russell Shomberg, Michael Jakuba, and Dana Yoerger. “Feasibility of a Near-Surface Wave-Powered Profiling Float for Extended Fully Submerged Autonomous Deployments”. In: *OCEANS 2022, Hampton Roads*. IEEE. 2022, pp. 1–10.
- [26] B. R. Smith. “The quadratically damped oscillator: A case study of a non-linear equation of motion”. In: *American Journal of Physics* 80.9 (2012), pp. 816–824.

- DOI: 10.1119/1.4729440. eprint: <https://doi.org/10.1119/1.4729440>. URL: <https://doi.org/10.1119/1.4729440>.
- [27] Leslie M Smith et al. “The ocean observatories initiative”. In: *Oceanography* 31.1 (2018), pp. 16–35.
 - [28] Robert H Stewart. *Introduction to physical oceanography*. Robert H. Stewart, 2008.
 - [29] Han Xiao et al. “Study of a novel rotational speed amplified dual turbine wheel wave energy converter”. In: *Applied Energy* 301 (2021), p. 117423.
 - [30] Ruijiang Xu et al. “Recent Progress on Wave Energy Marine Buoys”. In: *Journal of Marine Science and Engineering* 10.5 (2022), p. 566.